Characterization and Structural Studies of the Plasmodium Falciparum Ubiquitin and Nedd8 Hydrolase UCHL3

Characterization and structural studies of the *Plasmodium falciparum* ubiquitin and Nedd8 hydrolase UCHL3

Artavanis-Tsakonas, Katerina*[1], Weihofen, Wilhelm A*[2], Antos, John M[1], Coleman, Bradley I[3], Comeaux, Christy A[3], Duraisingh, Manoj T[3], Gaudet, Rachelle[2], Ploegh, Hidde L[#1]

[#] Corresponding author: ploegh@wi.mit.edu

* These authors contributed equally

[1] Whitehead Institute for Biomedical Research, Nine Cambridge Center, Cambridge, MA 02142, USA

[2] Department of Molecular and Cellular Biology, Harvard University, 7 Divinity Avenue, Cambridge, MA 02138, USA

[3] Harvard School of Public Health, Building I, 665 Huntington Avenue, Boston, MA 02115, USA

running title: PfUCHL3 characterization and crystallization

Summary

Like their human hosts, *Plasmodium falciparum* parasites rely on the ubiquitin-proteasome system for survival. We previously identified PfUCHL3, a deubiquitinating enzyme, and here we characterize its activity and changes in active site architecture upon binding to ubiquitin. We find strong evidence that PfUCHL3 is essential to parasite survival. The crystal structures

of both PfUCHL3 alone and in complex with the ubiquitin-based suicide substrate UbVME suggest a rather rigid active site crossover loop that likely plays a role in restricting the size of ubiquitin adduct substrates. Molecular dynamics simulations of the structures and a model of the PfUCHL3-PfNedd8 complex allowed the identification of shared key interactions of ubiquitin and PfNedd8 with PfUCHL3, explaining the dual specificity of this enzyme. Distinct differences observed in ubiquitin binding between PfUCHL3 and its human counterpart make it likely that the parasitic DUB can be selectively targeted while leaving the human enzyme unaffected.

Introduction

The regulation of protein function, localization, or degradation involves the action of specific hydrolases targeting ubiquitin (Ub) and ubiquitin-like protein (UBL) such as Nedd8. For ubiquitin, this family of hydrolases is collectively referred to as deubiquitinating enzymes (DUB). While intracellular apicomplexan parasites require their own self-encoded UBLs for survival, they may also encode agents capable of hijacking host UBL machinery. Although both viruses and bacteria lack the complete Ub machinery of their own, they do encode Ub ligases and proteins with de-ubiquitinating activity which may be used for interaction with their host, as well as for host-targeted, immune evasion (1). Although there is little direct evidence that the livelihood of eukaryotic parasites is dependent on UBLs, it is axiomatic that they use Ub and other Ub-like modifiers to regulate their physiology. Studies have reported a lethal effect on malaria parasites following treatment with proteasome inhibitors (2, 3). Therefore, parasitic UBL-regulating enzymes present interesting candidates for biological manipulation. Components of the Ub cascade have been successfully targeted in treatment of cancer (4); while these components have orthologs in parasitic pathogens, they show only moderate identity to their host counterparts, which makes them potential drug targets for apicomplexan-caused diseases such as malaria and toxoplasmosis. Indeed, the susceptibility

of *Plasmodium* to the antimalarial drugs chloroquine and artesunate have been linked to mutations mapping to a DUB locus in the mouse malaria model *P. chabaudi* (5). Furthermore, Ub-conjugating enzymes are upregulated in the death response of *Plasmodium* parasites as induced by treatment with antifolates (6). While these studies present interesting links between the Ub pathway and parasite survival, the molecular mechanisms which underlie them are not understood.

Profiling by activity based UBL-probes has facilitated the identification of DUBs, deNeddylases and deSUMOylating enzymes in a variety of organisms (7-9). PfUCHL3, the *Plasmodium* ortholog of mammalian UCHL3, was identified as part of such a screen in *P. falciparum* (10). Endpoint reactions with mammalian-derived UBL probes identified PfUCHL3 as a dual deNeddylase/DUB, consistent with the activity of its mammalian ortholog. Interestingly, a search by sequence homology for known deNeddylases fails to identify orthologs in *Plasmodium*, with the notable exception of UCHL3. That other non-orthologous enzymes function to remove Nedd8 from target proteins in *Plasmodium* is plausible (7), but PfUCHL3 may well play a larger and more central role in parasite physiology.

Here we characterize PfUCHL3 activity and changes in architecture upon Ub binding. We find strong evidence that PfUCHL3 is essential for parasite survival. To elucidate the structural basis for its dual Ub and Nedd8 specificity, we determined the crystal structures of PfUCHL3 free and in complex with the Ub-based suicide substrate UbVME. Molecular dynamics simulations of the determined structures and a model of the PfUCHL3-PfNedd8 complex identified shared key interactions between Ub/PfNedd8 and PfUCHL3, explaining the dual specificity of this enzyme. Distinct differences in the Ub binding site between PfUCHL3 and its human counterpart suggest that the parasitic DUB can be selectively targeted by inhibitors.

Results

Assessment of PfUCHL3 as a *P. falciparum*-specific deNeddylase

Previous work demonstrated that PfUCHL3 could react with Ub and Nedd8 probes, but not a SUMO probe (10). The probes used to identify PfUCHL3 were derived from the mouse Ub and Nedd8 sequences and have been characterized extensively (11). Briefly, these probes consist of the UBL equipped with an electrophilic warhead on the carboxy-terminus, capable of forming a covalent bond with the active site cysteine of target enzymes. Mouse and *Plasmodium* Ub are virtually identical, differing in only a single amino acid (E16D). The Nedd8 sequences, however, share only 52% amino acid identity (Figure 1A). Since mammalian Nedd8 is actually more similar to Ub than to PfNedd8 by sequence comparison (12), it was important to verify that PfUCHL3 reactivity toward PfNedd8 was real. To demonstrate that PfUCHL3 functions as a true deNeddylase in *Plasmodium* parasites, an electrophilic probe was generated in the form of a vinyl methyl ester added to the carboxy-terminus of N-terminally FLAG tagged PfNedd8. To increase solubility, four amino acids predicted to contribute to hydrophobic surface patches and located on the side opposite to the predicted PfUCHL3 binding site were changed to glutamines (Figure 1A and 1B). The resulting probe was reacted with *in vitro* translated PfUCHL3 yielding an N-ethyl maleimide (NEM)-sensitive 10 kDa shift in electrophoretic mobility (Figure 1C). This shift is the result of covalent attachment of the electrophilic PfNedd8 probe to PfUCHL3, thus establishing activity of the enzyme toward PfNedd8. Of note, previous work demonstrates that the probe indeed targets the PfUCHL3 active site cysteine (10). As further evidence, we observed similar shifts in electrophoretic mobility using probes derived from known substrates of PfUCHL3, including mammalian Nedd8 (MmN8-VS) and Ub (HAUb-VME). Whereas the PfNedd8 and Ub probes were used at saturating concentrations, the MmNedd8-VS concentration was sub-optimal, leading to incomplete conversion of enzyme to the covalent adduct.

Since the *in vitro* experiment shown in Figure 1C measures an endpoint reaction, the real-time kinetics of PfUCHL3 were also measured to ensure that UBL recognition and cleavage occur at a physiologically relevant rate. We first determined the steady-state kinetic parameters of PfUCHL3 for the hydrolysis of Ub-AMC (7-acetoxy-4-methyl coumarin) to KM = 301 nM and kcat = 3.2 s-1 for PfUCHL3, which are similar to those obtained for the human isofom (KM = 162 nM and kcat = 2.9 s-1, data not shown). Pf-UCHL3-mediated Nedd8-AMC hydrolysis was assessed and compared with that of HsUCHL3, an efficient DUB and deNeddylase (13) and NedP1, previously shown to be an efficient deNeddylase but not a DUB (14) (Figure 1D and 1E). AMC hydrolysis time-frames and efficiencies of PfUCHL3 were comparable to the positive controls for both Ub-AMC and Nedd8-AMC, thereby demonstrating that PfUCHL3 is truly bi-specific.

PfUCHL3 is likely essential to parasite growth and survival

In order to assess whether disruption of functional PfUCHL3 expression has an effect on parasite viability, a catalytically dead form of the enzyme was transfected into parasites in parallel with wild-type. PfUCHL3 was amino-terminally tagged with HA and this fusion was subsequently used as template to generate a cysteine to alanine substitution in the catalytic triad by site-directed mutagenesis. As previously demonstrated (10), this exchange renders the enzyme entirely inactive. HA-PfUCHL3wt and HA-PfUCHL3(C92A) were transfected into 3D7 parasites in parallel on three separate occasions. In each case, the HA-PfUCHL3wt parasites grew and expressed functional HA-PfUCHL3 (Figure 2A and B) whereas the mutants did not. These results suggest that the inactive enzyme is having a dominant negative effect on the endogenous wild type isoform and leads to the conclusion that this enzyme is likely essential to parasite survival.

Crystal structures of PfUCHL3 alone and in complex with Ub

To further probe the interaction of PfUCHL3 with its UBL substrates, structural studies were undertaken. The crystal structure of HsUCHL3 has been determined both in its free form (15) as well as in complex with Ub (16), both of which served as references for PfUCHL3. An amino acid sequence alignment of the human and *P. falciparum* enzymes, which are 30% identical, is shown in Figure 3A.

The crystal structure of the PfUCHL3-UbVME complex (Figure 4A) was determined by molecular replacement using the components of the structure of human UCHL3 bound to UbVME (pdb code 1xd3) as search models. The structure was refined to a resolution of 2.3 Å and a final R_{work} value of 18.8 % (R_{free} 23.5 %). The refined PfUCHL3 structure was in turn used as a search model in molecular replacement to determine the 2.4 Å resolution structure of free PfUCHL3 (Figure 3C; R_{work} 21.8 % and R_{free} 25.1 %). See Table 1 for data collection and refinement statistics.

Continuous electron density was observed for all Ub residues, whereas for both UbVME-bound and free PfUCHL3 the four N-terminal residues and residues 58 to 78, corresponding to helix 3 in HsUCHL3, lack interpretable density and are therefore disordered. Like its human ortholog, the PfUCHL3 structure is composed of a helix-β-helix sandwich that features a central six-stranded anti-parallel β-sheet surrounded by seven α-helices (Figures 4A and B). The C-terminus of UbVME binds a narrow groove lined by the catalytic triad residues Cys92, His164, and Asp179. The UbVME C-terminal tail is also covered by the PfUCHL3 crossover loop (Figure 4A). Electron density for the active site shows the catalytic cysteine, located at the N-terminus of central helix 4, participating in a 1.7 Å thioether bond with the VME moiety that replaces the C-terminal G76 of wild type Ub (Figure 5B). In addition to the interactions between the Ub C-terminus and active site residues, conserved residues Y35 and L41 of PfUCHL3 that precede helix 2 cover a hydrophobic surface patch on the Ub β-sheet. Finally, the first β-hairpin loop of Ub, with residues L8 and T9 (both are conserved in Nedd8 but in no other UBL), is accommodated by a narrow hydrophobic pocket lined by Helix 7 and the loop preceding Helix 1, a signature

interaction motif between UCH family proteases and Ub (Figure 4).

Conformational changes between free and Ub-bound UCHL3

As expected, a DALI database search identified the closest structural neighbors of PfUCHL3 as human UCHL3 and UCHL1 and yeast UCH (Yuh-1). The sequence identities of these enzymes exceed 28% and superimpositions of at least 190 Cα atoms yielded root mean squared deviation (rmsd) values below 2.2 Å. The structural similarities of PfUCHL3, HsUCHL3 and Yuh-1 suggest a shared mode of Ub recognition (Figures 4A and B and data not shown). However, the free forms of the respective enzymes each exhibit distinct features. For instance, helix 6' and the following crossover loop region are disordered in free HsUCHL3 (Figure 4B). Furthermore, the groove that accommodates the C-terminal stretch of Ub is partly occluded by a loop requiring major conformational changes upon binding of Ub or Nedd8 (15, 16). On the other hand, the free HsUCHL1 crystal structure shows the crossover loop in a distinct conformation but the Ub binding site and catalytic triad residues are not aligned to form a functional proton relay system, a possible explanation for the low *in vitro* catalytic activity of UCHL1 (17). In contrast, free PfUCHL3 features an ordered crossover loop and the catalytic triad residues are within hydrogen bonding distance of each other. Upon UbVME binding, PfUCHL3 undergoes small conformational changes within all loop elements that contact UbVME (Figure 4C). These loop regions of free and UbVME-bound PfUCHL3 show an rmsd of 2.4 Å, whereas the remaining portions of the molecule superimpose well with an rmsd of 0.5 Å. The fact that the crossover loop is ordered in the structure of free PfUCHL3 is likely due to crystal contacts in this region, locking the loop in a distinct conformation. Nevertheless, the lack of significant structural changes upon Ub binding suggests that the crystal contacts do not extensively deform or displace the crossover loop (Figure 4C). It has been proposed that unfolding of Helix 6' and a significant displacement of the loop is required to allow binding of Ub ligated to larger substrates, and that the crossover loop then folds back to induce hydrolysis of the active site cysteine-Ub

thioester intermediate after isopeptide bond hydrolysis (16). However, when the crossover loop was cleaved or extended by insertion of up to ten glycine residues, UCHL3 hydrolyzed diUb linkages much more efficiently (18). This observation supports the notion that UCHL3's main function is to free Ub from adducts with small molecules and not the cleavage of Ub linked to large, globular proteins. In PfUCHL3, Helix 6' forms a large hydrophobic interface and is tightly bound to the enzyme core. Therefore, we do not expect that this helix readily unfolds in the free form as observed for HsUCHL3. This is supported by the fact that in molecular dynamics simulations (discussed below), Helix 6' did not exhibit significant flexibility or conformational changes within the timeframe of the simulation.

Interactions of PfUCHL3 with the Ub C-terminus

As observed in other DUBs, the C-terminal ^{71}LRLRG^{75} motif of Ub adopts an extended β-sheet conformation, with the backbone carbonyl and amide groups forming an intimate hydrogen-bonding network to the PfUCHL3 residues that line the interface (Figure 5A). The side chain of R72 forms a salt bridge to PfUCHL3 D33, a conserved residue and interaction described in related UCHL3/Yuh-1-Ub complexes (16). The sequence of the crossover loop is not conserved between human and PfUCHL3 (Figure 3A). As a result, the crossover loops of the respective enzymes do not share the same conformation and interaction pattern with Ub (Figure 4B). In particular, D157 located within the loop of PfUCHL3 forms a salt bridge to the side chain of R74 of Ub, which in turn forms a hydrogen bond to the side chain of Q151 (Figure 5A). Residues L71 and L73 point to the opposite wall of the groove and occupy a hydrophobic binding pocket.

Despite the overall similarity of the Ub recognition and binding mode between *P. falciparum* and human UCHL3, the interfaces with Ub of both enzymes feature notable differences; the most significant ones are illustrated in Figure 5A. In the Ub-binding groove of PfUCHL3, S12 (A11 in HsUCHL3) forms an additional hydrogen bond to the backbone nitrogen of Ub

L73. PfUCHL3 residues therefore satisfy all hydrogen bond donors and acceptors of Ub C-terminal residues 71-75. The highly conserved Ub R74, a key residue for Ub recognition, forms an intricate network of hydrogen bonds with HsUCHL3 residues, but adopts a different conformation and is implicated in an altogether different set of hydrogen bonds to PfUCHL3 residues. For instance, a salt bridge is formed to D157, which is located in the crossover loop region. Finally, non-conserved residues T163 and S219 (L168 and N223 in HsUCHL3, respectively) complete the interface of PfUCHL3 with Ub (Figure 5A).

Molecular dynamics (MD) simulations of a PfNedd8 model in complex with PfUCHL3

Although we were able to generate milligram amounts of pure and monodisperse PfUCHL3-PfNedd8VME complex, attempts to crystallize the complex have thus far failed to yield crystals. To better understand the interaction of PfNedd8 with PfUCHL3, we generated a homology model of PfNedd8 threaded onto the crystal structure of free Ub (pdb code 1ubq), then docked this model into the Ub/Nedd8 binding site of PfUCHL3. As shown in Figure 3B, essentially all Ub residues that interact with PfUCHL3 in the complex are identical in PfNedd8 except for I70, which corresponds to V70 in Ub, a conservative substitution, and K39, which corresponds to D39 in Ub and is located at the periphery of the interface. Our modeling results suggest that PfNedd8 K39 could form a salt bridge to E153 of PfUCHL3. For the MD simulations, the PfNedd8 model was equipped with the natural C-terminal glycine, representing a post-hydrolysis state. This complex was equilibrated for 10 ns in molecular dynamics simulations at 37 °C using NAMD and the CHARMM22 force field (see methods for references). The PfUCHL3-Ub complex, also with a C-terminal glycine, was simulated for 5 ns and served as a reference for comparison of any structural changes during the simulations. Within the timeframe of the simulations we did not observe a dissociation of either Ub or Nedd8; there was no significant increase in the distance between the centers of mass of the protease and substrate at any time point of the simulation. However, the modeled PfNedd8 exhibited a steady drop in the average rmsd from 2 to 1 Å within the first 2 ns of

simulation, indicating that the PfNedd8 model based on threading changed its conformation to reach an energetic minimum (Figure 6A). Figure 5B shows snapshots after 5 and 10 ns of simulation for PfUCHL3 in complex with Ub and PfNedd8, respectively. Notably, R74 of both Ub and PfNedd8 form a salt-bridge to D157 within the crossover loop region of PfUCHL3 after ~2 ns of the simulation, an arrangement that contrasts the conformation and coordination by hydrogen bonds of R74 in the crystal structure of the complex (compare R74 in Figures 5A and 6B, Supplementary Movie 1). Of note, in the crystal structure the crossover loop participates in crystal contacts and thereby may have restricted the positioning of D157 and prevented its interaction with R74 in the favored conformation revealed by the simulations. Furthermore, the simulation of PfUCHL3-PfNedd8 shows that Q72 of PfNedd8 (R72 in Ub) readily forms hydrogen bonds to E11 and N13 of PfUCHL3. The consistent results for the simulations of PfUCHL3 with either Ub or PfNedd8 suggest that the identified favorable interactions between PfNedd8 and PfUCHL3 likely represent natural interactions between these elements. In summary, the modeling and MD simulations provide additional support that PfNedd8 is a natural substrate of PfUCHL3.

The MD simulations can also provide information about the flexibility of the PfUCHL3-Ub complex. In the HsUCHL3-UbVME crystal structure, structural differences between two complexes in the asymmetric unit suggested that HsUCHL3 and UbVME do not form a rigid complex assembly. Rather, Ub is allowed rotational freedom of ~10° relative to HsUCHL3 (16). In the PfUCHL3-UbVME crystal structure, the asymmetric unit also contains two complexes that are structurally very similar, as reflected by an rmsd of 0.3 Å for all Cα atoms. Further examination of the crystal lattice indicates that the high degree of similarity stems from the fact that the two PfUCHL3-UbVME complexes are in fact related by a pseudo-twofold axis, and they therefore have very similar crystal contacts. This pseudo-twofold symmetry thus prevents the use of the two observations of the PfUCHL3-UbVME complexes to assess the possible rotational freedom of Ub as observed in

the crystal structure of UbVME bound to HsUCHL3. However, the extent of rotational freedom of Ub when bound to PfUCHL3 could be derived from the MD simulations and we observed a rotation hinged around residue R72 of Ub, with a maximal displacement of ~9˚ during the simulation. The MD simulations therefore indicate that the interaction of PfUCHL3 with Ub has flexibility similar to that previously observed for HsUCHL3 (16). Finally, we also performed a short 4 ns MD simulation of free PfUCHL3. This simulation revealed significant flexibility within the crossover loop region as reflected by rmsd values in the range of 5 Å (Supplementary Movie 1). This is consistent with structures of free HsUCHL3, UCHL1 and Yuh-1, in which the crossover loop shows significant flexibility or disorder. However, the loop and adjacent Helix 6' of PfUCHL3 did not readily unfold within the 4 ns timeframe of the simulation, suggesting that the crossover loop region is not inherently unstable in the free enzyme form. Its ordered conformation in the free PfUCHL3 is likely not just an artifact of crystal packing. As mentioned above, this is supported by the extensive hydrophobic interface between Helix 6' and the enzyme core.

Discussion

We previously identified PfUCHL3 as a functional DUB in *P. falciparum.* We now extend our study of this enzyme by characterizing its specificity and structure. We determined the crystal structures of both the Ub-liganded and free forms to gain insight into the architectural changes that occur upon substrate binding, and to establish how these changes differ from those of the human ortholog. We further establish the basis of this enzyme's dual specificity for both Ub and Nedd8 by identifying the key interactions between the enzyme and UBL residues.

The cross-over loop that obstructs access to the active site has been the subject of considerable study and speculation in regard to its function in conferring substrate specificity.

When the human enzyme was crystallized in an unliganded form (15), this loop was disordered, leading to the conclusion that it is flexible. Conversely, the loop adopted an ordered conformation when crystallized in complex with Ub (16). It was hypothesized that instead of simply limiting the size of substrates, the loop can rotate to allow catalysis of larger targets, although larger proteins have been found to be inefficiently deubiquitinated by UCHL3 (19). In the yeast Yuh-1 structure and in both the unliganded and complexed structures of PfUCHL3 presented here, this cross-over loop is ordered; crystal packing may at least partly contribute to their stabilization and these observations therefore are silent on the question whether or not the crossover loop in yeast and *Plasmodium* is rigid. A short MD simulation of the free PfUCHL3 shows significant motion of the loop, supporting the idea that it is at least somewhat flexible. An alternative hypothesis is that the cross-over loop functions to limit catalysis to small ubiquitinated substrates able to enter the narrow space between the catalytic site and the cross-over loop, thereby directly functioning to define enzyme specificity. By artificially extending the loop by 5-10 residues, the specificity of both *Plasmodium* and human UCHL3 can be altered to cleave bulky substrates, which neither wild type enzyme is able to do (18). In light of this recent study, it seems more plausible that the loop indeed limits UCHL3 DUB and deNeddylase activity to small substrates, a point which will inevitably become clearer as specific substrates are defined in both the parasite and human host.

Structurally, the PfUCHL3/Ub adduct presented here is very similar to the Ub adduct with the human ortholog (16), as well as to the yeast Yuh-1/Uba-1 complex (20). Despite their structural similarities, however, PfUCHL3 apparently fulfills a more central functional role than its human and yeast counterparts. Disruption of the UCHL3 gene in mice and of Yuh-1 in yeast leaves viability unaffected and more generally yields no major discernible phenotypes. In both cases, it is hypothesized that other DUBs and deNeddylases can compensate. In *P. falciparum*, PfUCHL3 is the only deNeddylase present in the genome (as determined by sequence homology to known human deNeddylases) and when a catalytically

inactive version of the enzyme is transgenically over-expressed in parasites, a dominant negative effect prevails and inhibits parasite growth.

Nedd8 has been implicated in cell cycle control, specifically in the progression from G1 to S phase. Interfering with the Nedd8 pathway in hamster cells results in these cells bridging multiple S phases while failing to undergo mitosis (21). Given the highly conserved nature of the UBL pathways across evolution, it is reasonable to assume that PfNedd8 also plays an essential role in maturation, controlling progression throughout the divergent and specialized stages of the parasite's erythrocytic cycle. Disrupting this cycle, by ways of interfering with the enzyme responsible for processing the PfNedd8 pro-protein, should have devastating effects on viability.

The identification of selective inhibitors to PfUCHL3 would not only facilitate the further characterization of this enzyme *in vivo* and *in vitro*, but could also potentially provide a novel class of therapeutics with which to combat parasitic diseases. Inhibitors would need to be eliminated based on cross-reactivity with host proteins. This has been a challenge in specifically targeting the *Plasmodium* proteasome with small molecules whilst at the same time avoiding off-target effects on the human homologous complex. PfUCHL3 provides a promising target, given the architecture of the active site we present here and the identified differences with the catalytic site of the human ortholog. Indeed, HsUCHL3 and UCHL1, which are closely related and share a higher level of sequence similarity than the human and *Plasmodium* UCHL3 (53% and 35.9%, respectively), can be selectively targeted by small molecules with μM differences in inhibitory capacity (22). The structures for the liganded and unliganded forms of PfUCHL3 and of the modeled residue contacts between the enzyme and PfNedd8 should facilitate exploratory chemistry to identify inhibitors and put such efforts on a solid molecular footing. In turn, manipulation of PfUCHL3 will allow further characterization of both the Ub and Nedd8 pathways in *Plasmodium* and a better understanding of how they have diverged from those of the human host and can be effectively targeted for therapeutic purposes.

Experimental Procedures

Generation of electrophilic probes

Probes were generated as described in (8) *P. falciparum* FLAG-Nedd8 could not be expressed in soluble form. Four mutations were introduced using site-directed mutagenesis (Quickchange Kit, Stratagene) to exchange hydrophobic residues to glutamines, namely F24Q, M28Q, M54Q and V62Q. Subsequently, FLAG-PfNedd8-VME was generated as previously described (8). Briefly, PfFLAGNedd8 was cloned into the pTYB4 vector (NEB) and expressed as a fusion with a carboxy-terminal intein and chitin binding domains in BL21-CodonPlus (DE3)-RIL competent cells (Stratagene) and induced with 1 mM IPTG for 4 hours at 30 °C. Fusions were purified using chitin beads (NEB), eluted by forcing intein excision with beta-mercaptoethane sulfonic acid and subsequently modified in the presence of NHS and glycine-vinyl methyl ester (VME) to yield active probes.

In vitro translation

PfUCHL3 was previously cloned into pcDNA (10). *In vitro* coupled transcription/translation was performed in the presence of ^{35}S cysteine-methionine and reacted with PfFLAGNedd8-VME, HAUb-VME or MmNedd8-vinyl sulfone (VS) for 2 hours at room temperature in the presence or absence of N-ethyl maleimide (NEM). Polypeptides and complexes were visualized by SDS-PAGE and autoradiography as previously described (10).

Maintenance of parasite cultures

The 3D7 strain of *P. falciparum* was obtained from the WEHI (Melbourne, Australia), and the 3D7-attB strain was obtained from the Fidock lab at Columbia University (New York, USA).

Both were maintained in *in vitro* culture as previously described (23). Briefly, parasites were cultured in human O+ erythrocytes at 4% hematocrit in RPMI-1640 medium (Sigma) supplemented with 25 mM HEPES (EMD Biosciences), sodium bicarbonate (Sigma), 50 mg/L hypoxanthine (Sigma), and 0.5% Albumax II (Invitrogen).

Generation of transgenic parasite lines

The PfUCHL3 wild type gene was amplified by PCR from *P. falciparum* cDNA and subcloned into a pUML vector as a fusion with a carboxy-terminal triple HA tag under control of the *P. falciparum* calmodulin promoter. To generate transgenic parasite strains, sorbitol-synchronized ring-stage parasites at 5-10% parasitemia were transfected with ~100 plasmids/cell by electroporation. Positive transfectants were selected by treatment with 2.5nM WR99210 (24, 25). The presence of the episome in this strain was maintained by continuous culture on 2.5 nM WR99210.

Southern blot analysis

Genomic DNA was harvested from synchronous, late-stage parasite cultures using the QIAamp DNA Mini Isolation Kit (QIAGEN). For the PfUCHL3wt-3HA transfection, the presence of episome in recovered parasites was assessed by Southern blot using standard procedures. The southern probe was a PCR product corresponding to the entire cDNA sequence of PfUCHL3, and was generated with the same primers used for cloning the PfUCHL3 coding sequence.

Western blot analysis

Expression and reactivity of the modified enzyme were verified by Western blot. Mixed stage parasites were lysed using 1% NP-40 in the presence of protease inhibitors (Roche) and lysate (40 μg protein) was incubated for an hour at room temperature in the presence or absence of Ub-VME and subsequently separated by SDS-PAGE. Polypeptides were

transferred onto PVDF membranes which were probed with 3F10-HRP (Roche) to visualize HA-reactive proteins by chemiluminescence. PfUCHL3 expression was determined by the appearance of an HA-reactive band of the expected mass and enzyme reactivity by the shift of this band by 9kDa to reflect covalent modification by Ub-VME.

Expression and purification of Hs and PfUCHL3

HsUCHL3 was generated as previously described (18). PfUCHL3 was cloned into the pET28(a)+ vector in frame with an N-terminal 6xHis tag. BL21-CodonPlus (DE3)-RIL competent cells were transformed with plasmid DNA and protein expression was induced with 1 mM IPTG for 3 hours at 30 °C. Initial purification was done on Ni-NTA beads (Qiagen) and the His-tag was removed by thrombin cleavage using thrombin-agarose following the manufacturer's specifications (CleanCleave Kit, Novagen). Further purification was done by size exclusion chromatography (S75 10/30, GE Healthcare) run with 25 mM Tris/HCl, 200 mM NaCl, 10 mM DTT and 2 mM EDTA, pH8.0. Fractions with an apparent MW of 30 kDa that corresponds to monomeric PfUCHL3 were concentrated to 10 mg/mL and subsequently used in crystallization trials.

AMC assays

Ub-AMC (Ub C-terminal 7-amido-4-methyl coumarin) and Nedd8-AMC hydrolysis assays were performed as described previously (26). Briefly, the hydrolysis was performed in reaction buffer (50 mM Tris/HCl, 150 mM NaCl, 2 mM EDTA, 2 mM DTT [pH 7.5]) supplemented with 0.1 mg/ml of bovine serum albumin (BSA) (Pierce). PfUCHL3 and HsUCHL3 concentrations were determined by Bradford test using BSA as a standard. NedP1, Ub-AMC and Nedd8-AMC were purchased from Boston Biochem.

Crystallization and adduct formation

Crystals of free PfUCHL3 grew from sitting drops at 4 ºC in conditions containing 100 mM

Bicine, 25 % PEG 2000, 15 % glycerol, 300 mM $MgCl_2$, pH 9.0 as thin plates with maximal dimensions of 0.3x0.2x0.03 mm^3. For cryoprotection, crystals were incubated in reservoir solution supplemented with glycerol in increments of 5 % from of 5 to 20 % (v/v) prior to flash freezing crystals in liquid N_2.

To prepare the covalent complex, PfUCHL3 was reacted with a molar excess of Ub-vinyl methyl ester (UbVME) at room temperature for 2 hr. The complex was separated from unliganded PfUCHL3 by anion exchange chromatography on MonoQ resin (GE Healthcare). Proteins were eluted by applying a 10 to 300 mM NaCl gradient in 50 mM TrisHCl pH 7.5, 3 mM DTT, 1 mM EDTA. Fractions containing PfUCHL3-UbVME were concentrated to 10 mg/mL and used in crystallization trials. Crystals of the complex grew at 20 ºC from a condition containing 100 mM Bis-Tris pH 5.5, 200 mM NaCl, 25% PEG 3350 to maximal dimensions of 0.05x0.05x0.1 mm^3. Crystals were soaked in crystallization solution supplemented with 20 % glycerol (v/v) prior to flash freezing in liquid N_2.

X-ray data collection and structure determination

X-ray diffraction data of PfUCHL3-UbVME crystals were collected at 100 K at NE-CAT beamline ID24 at the Advanced Photon Source, Argonne IL, and processed with HKL2000 (27). The crystal structure of PfUCHL3-UbVME was determined by molecular replacement with PHASER (28) using the components of the HsUCHL3-UbVME structure as search models (pdb code 1XD3). The model was built in coot (29) and refined with REFMAC5 (30). A 2.5 Å resolution data set from a free PfUCHL3 crystal was collected in house at 100 K using a MicroMax-007 rotating anode generator and R-AxisIV++ detector (Rigaku/MCS Inc). Data were processed with HKL2000. The structure of PfUCHL3 in complex with UbVME was used as a search model in PHASER and the structure refined with REFMAC5 (30).

Data collection and refinement statistics are summarized in Table 1. Model quality was assessed using WHAT_CHECK (31), showing that all φ, ψ are within the allowed regions of

the Ramachandran plot for the complex structure of PfUCHL3-UbVME and few are within generously allowed regions for the structure of free PfUCHL3.

Molecular dynamics simulations

VMD (32) was used to build three systems containing free PfUCHL3 (Protein Data Bank code 2we6), PfUCHL3-Ub (Protein Data Bank code 2wdt) with the VME moiety replaced by the natural G76, and a model of PfUCHL3-PfNedd8 based on the Ub crystal structure (pdb code 1ubq) built using SwissModel (33). All three systems were solvated in water with sodium and chloride ions randomly placed for cell neutralization.

The resulting free PfUCHL3, PfUCHL3-Ub and PfUCHL3-Nedd8 systems contained a total of 65840 atoms (121 ions), 76041 (134 ions) and 73278 (132 ions), respectively. Asp, Glu, Lys, and Arg residues were assumed to be charged throughout, while the protonation states of His residues were chosen to favor the formation of evident hydrogen bonds. All molecular dynamics simulations were performed using NAMD 2.6 (34), the CHARMM22 force field for proteins with the CMAP correction (35), and the TIP3P model for water (36).

A uniform integration 2-fs time step was assumed for all types of interactions throughout all simulations. A 12-Å cutoff was applied with a switching function starting at 10Å for van der Waals interactions, and the particle-mesh-Ewald method (with grid point density at least 1 $Å^{-3}$) was used to compute long-range electrostatic forces without cutoff (37), with a grid point density of at least 1 $Å^{-3}$. Langevin dynamics were used to maintain a constant temperature of 310 K, with the damping coefficient set to 0.1 ps^{-1} for all heavy atoms. Coordinates of all atoms of the system were saved every ps for later analysis. Overall structural changes of the proteins were monitored with VMD by computing rmsd values of Cα atoms over the entire trajectories, using the crystallographic structure (or starting homology model in the case of the PfNedd8 complex) as a reference point.

Acknowledgements

The authors would like to thank Stephen Harrison, David Fidock, Rich Eastman, Max Popp and Marcos Sotomayor for helpful discussions. The authors state no conflicts of interest.

Figure legends

Figure 1. Both mammalian and *P. falciparum*-derived Nedd8 are substrates for PfUCHL3.

(A) Sequences of the *P. falciparum* and human Nedd8 orthologs were aligned to show the 52% identity between the two proteins. Residues mutated to glutamine to achieve solubility in protein expression experiments are marked with an asterisk (*).

(B) The four side chains mutated to glutamine are shown in gray on a ribbon model of PfNedd8. (C) To show that PfUCHL3 is specific for PfNedd8, the parasite UBL (with the four solubilizing mutations) was N-terminally FLAG-tagged and modified with a vinyl methyl ester (VME) on its carboxy-terminus to generate an active electrophilic probe. PfUCHL3 was expressed using *in vitro* coupled transcription/translation in the presence of ^{35}S methionine, and subsequently reacted with FLAG-PfNedd8-VME, mammalian Nedd8-vinylsulfone (MmNedd8-VS) or hemagglutinin-tagged ubiquitin vinyl methyl ester (HAUb-VME) in the presence or absence of 10mM NEM to show cysteine-specific activity and analyzed by SDS-PAGE followed by autoradiography. A shift in molecular weight in the absence of NEM demonstrates reactivity.

(D-E) Assays based on enzymatic cleavage of Ub-AMC and Nedd8-AMC show that PfUCHL3 substrate recognition happens at physiologically relevant rates when compared to HsUCHL3 and NedP1. Each enzyme was mixed with an excess of Ub-AMC (D) or

Nedd8-AMC (E) substrate. Cleavage was measured by fluorescence output every 2 minutes for a total of 40 minutes.

Fig. 2. HA-PfUCHL3wt-expressing parasites are viable and express functional enzyme. Transgenic, HA-PfUCHL3-expressing parasites were tested by Southern blot to verify transgene presence (A). Genomic DNA from 3D7 wildtype and PfUCHL3 transgenic parasites digested with AccI/PacI and hybridized with a ^{32}P-labeled probe representing the PfUCHL3 sequence. Presence of the episome containing the exogenous PfUCHL3 ORF shown by a hybridization signal of 6033bp. The stronger signal from the episome signifies multiple copies of the overexpression plasmid. (B) Crude parasite lysates derived from the untransfected parent line (WT) and the transgenic line (PfUCHL3) were reacted with Ub-VME and blotted with anti-HA.

Figure 3. Sequence alignments of *P. falciparum* and human UCHL3, and PfNedd8 with Ub. (A) The aligned PfUCHL3 and HsUCHL3 amino acid sequences. The parasitic enzyme sequence was previously determined (10). Catalytic triad residues are marked by asterisks (*) and the sequence corresponding to the cross-over loop is boxed. (B) The PfNedd8 sequence was aligned with that of human Ub. PfUb and HsUb and differs at a single amino acid (residue 16 is E or D in human or *P. falciparum*, respectively). Reagents based on the HsUb were used throughout these experiments. In both alignments, black boxes indicate identical residues and white boxes, conservative substitutions.

Figure 4. Crystal structures of free PfUCHL3 and the PfUCHL3-UbVME complex. **(A)** Ribbon representation of the PfUCHL3 structure (grey) in complex with UbVME (green). Side chains of the catalytic triad residues are shown in yellow. The dashed line represents a disordered region spanning residues 58-78.
(B) Superimposition of the UbVME complex of HsUCHL3 (orange) and PfUCHL3 (grey).

Only one bound UbVME (green), that of PfUCHL3, is shown for clarity. The disordered region of PfUCHL3 corresponds to Helix H3 in HsUCHL3. The crossover loop of both structures adopt notably different conformations. In the crystal structure of free HsUCHL3, this loop and Helix 6' were unstructured (15).
(C) Structure of free PfUCHL3 (blue) superimposed onto UbVME-bound PfUCHL3 (grey). Loop regions implicated in Ub recognition are indicated by arrows and undergo significant conformational changes upon Ub binding.

Figure 5. Interface between the Ub C-terminus and the active site of PfUCHL3.
(A) Interactions of the extended C-terminus of Ub (green) with PfUCHL3 residues (grey) lining the narrow groove. The catalytic C92 forms a covalent bond to the VME moiety replacing the C-terminal G76 of Ub. Note that all backbone carbonyl and amide groups are coordinated by hydrogen bonds (dashed lines) to PfUCHL3 residues. Corresponding HsUCHL3 residues that are not conserved in PfUCHL3 are shown in orange. Hydrogen bonds only observed in the PfUCHL3-UbVME complex are shown as dashed green lines.
(B) 2Fo-Fc electron density map contoured at 1.3 σ indicates a covalent bond between the catalytic cysteine C92 and the former VME moiety at the Ub C-terminus.

Figure 6. Molecular dynamics simulations of PfUCHL3-PfNedd8.
(A) Root mean-square deviations for PfUCHL3 in complex with Nedd8. RMSD of Cα atoms were computed throughout a 10 ns simulation for the complex (green curve) and components Nedd8 (red curve) and PfUCHL3 (black curve). RMSD for modeled Nedd8 reached stable values below 1 Å after 2 ns of simulation.
(B) Model of the PfUCHL3 active site bound to PfNedd8VME (magenta) after 10 ns of equilibration in MD simulations. The corresponding Ub C-terminal residues (green) as observed in the PfUCHL3 complex after being subjected to a similar simulation are

superimposed. The conformation of Ub residue R74 changes significantly during the simulation (compare to Figure 4A) and resembles that of Nedd8 R74, forming a salt bridge to D157. Simulations suggest that Nedd8 Q72 interacts with E11 and N13 of PfUCHL3.

Supplementary Movie 1. Molecular dynamics simulation of the structural model of PfUCHL3-PfNedd8. The extended C-terminus of PfNedd8 (magenta), modeled in a post-hydrolysis state, forms a stable complex in the active site groove of PfUCHL3 (grey) over the 10 ns simulation. Notably, the PfNedd8 R74 forms a salt-bridge to PfUCHL3 D157 within the crossover loop region of PfUCHL3 after ~2 ns of the simulation (bottom right).

Table 1. Crystallographic data and refinement statistics

	free PfUCHL3	**PfUCHL3-UbVME**
Space group	C2	$P2_12_12$
Unit cell parameters (Å) β angle (°)	168.3, 45.0, 99.5 121.8	134.3 75.3 85.6
Resolution range (Å)	28.2-2.42	20.0-2.30
Observed reflections	68,483	223,276
Unique reflections	24,494	38,252
Completeness (%)[a]	99.0 (96.2)	99.1 (97.6)
I/σ(I)	11.1 (2.3)	14.4 (2.1)
R_{sym} (%)[b]	7.5 (48.9)	9.3 (45.1)
Rr.i.m. (%)[c]	9.3 (59.3)	7.6 (47.3)
Rp.i.m. (%)[c]	5.4 (34.1)	2.9 (23.1)
Refinement Statistics		
Protein atoms Solvent atoms	3,394 123	4,549 189

R_{work} (%)	21.8	18.8
R_{free} (%)	25.1	23.5
RMS deviations[d]		
Bond lengths (Å)	0.011	0.013
Bond angles (°)	1.3	1.3
Ramachandran regions[e]		
Favoured (%)	96.3	97.8
Allowed (%)	3.7	2.2
Disallowed (%)	0.0	0.0

[a] Values in parentheses refer to the outer resolution shell
[b] $R_{sym} = (|I_{hkl} - \langle I \rangle|) / (I_{hkl})$, where I_{hkl} is the observed intensity and $\langle I \rangle$ is the average intensity obtained from multiple observations of symmetry-related reflections
[c] Computed with RMERGE (38)
[d] Computed with WHAT_CHECK
[e] Computed with MOLPROBITY (39)

References

1. Isaacson, M. K. and Ploegh, H. L. (2009) *Cell Host Microbe* **5**, 559-570
2. Featherstone, C. (1997) *Mol Med Today* **3**, 367
3. Lindenthal, C., Weich, N., Chia, Y. S., Heussler, V. and Klinkert, M. Q. (2005) *Parasitology* **131**, 37-44
4. Sun, Y. (2003) *Cancer Biol Ther* **2**, 623-629
5. Hunt, P., Afonso, A., Creasey, A., Culleton, R., Sidhu, A. B., Logan, J., Valderramos, S. G., McNae, I., Cheesman, S., do Rosario, V., Carter, R., Fidock, D. A. and Cravo, P. (2007) *Mol Microbiol* **65**, 27-40
6. Ganesan, K., Ponmee, N., Jiang, L., Fowble, J. W., White, J., Kamchonwongpaisan, S., Yuthavong, Y., Wilairat, P. and Rathod, P. K. (2008) *PLoS Pathog* **4**, e1000214
7. Artavanis-Tsakonas, K., Misaghi, S., Comeaux, C. A., Catic, A., Spooner, E., Duraisingh, M. T. and Ploegh, H. L. (2006) *Mol Microbiol* **61**, 1187-1195

8. Borodovsky, A., Ovaa, H., Kolli, N., Gan-Erdene, T., Wilkinson, K. D., Ploegh, H. L. and Kessler, B. M. (2002) *Chem Biol* **9**, 1149-1159
9. Misaghi, S., Balsara, Z. R., Catic, A., Spooner, E., Ploegh, H. L. and Starnbach, M. N. (2006) *Mol Microbiol* **61**, 142-150
10. Frickel, E. M., Quesada, V., Muething, L., Gubbels, M. J., Spooner, E., Ploegh, H. and Artavanis-Tsakonas, K. (2007) *Cell Microbiol* **9**, 1601-1610
11. Hemelaar, J., Borodovsky, A., Kessler, B. M., Reverter, D., Cook, J., Kolli, N., Gan-Erdene, T., Wilkinson, K. D., Gill, G., Lima, C. D., Ploegh, H. L. and Ovaa, H. (2004) *Mol Cell Biol* **24**, 84-95
12. Ponder, E. L. and Bogyo, M. (2007) *Eukaryot Cell* **6**, 1943-1952
13. Wada, H., Kito, K., Caskey, L. S., Yeh, E. T. and Kamitani, T. (1998) *Biochem Biophys Res Commun* **251**, 688-692
14. Shen, L. N., Liu, H., Dong, C., Xirodimas, D., Naismith, J. H. and Hay, R. T. (2005) *EMBO J* **24**, 1341-1351
15. Johnston, S. C., Larsen, C. N., Cook, W. J., Wilkinson, K. D. and Hill, C. P. (1997) *EMBO J* **16**, 3787-3796
16. Misaghi, S., Galardy, P. J., Meester, W. J., Ovaa, H., Ploegh, H. L. and Gaudet, R. (2005) *J Biol Chem* **280**, 1512-1520
17. Das, C., Hoang, Q. Q., Kreinbring, C. A., Luchansky, S. J., Meray, R. K., Ray, S. S., Lansbury, P. T., Ringe, D. and Petsko, G. A. (2006) *Proc Natl Acad Sci U S A* **103**, 4675-4680
18. Popp, M. W. (2009) *J Biol Chem* **284**, 3593-3602
19. Larsen, C. N., Krantz, B. A. and Wilkinson, K. D. (1998) *Biochemistry* **37**, 3358-3368
20. Johnston, S. C., Riddle, S. M., Cohen, R. E. and Hill, C. P. (1999) *EMBO J* **18**, 3877-3887
21. Lammer, D., Mathias, N., Laplaza, J. M., Jiang, W., Liu, Y., Callis, J., Goebl, M. and Estelle, M. (1998) *Genes Dev* **12**, 914-926
22. Mermerian, A. H., Case, A., Stein, R. L. and Cuny, G. D. (2007) *Bioorg Med Chem Lett* **17**, 3729-3732
23. Trager, W. and Jensen, J. B. (1976) *Science* **193**, 673-675
24. Fidock, D. A. and Wellems, T. E. (1997) *Proc Natl Acad Sci U S A* **94**, 10931-10936
25. Triglia, T., Wang, P., Sims, P. F., Hyde, J. E. and Cowman, A. F. (1998) *EMBO J* **17**, 3807-3815
26. Schlieker, C., Weihofen, W. A., Frijns, E., Kattenhorn, L. M., Gaudet, R. and Ploegh, H. L. (2007) *Mol Cell* **25**, 677-687
27. Otwinowski, Z. and Minor, W. (1997) *Methods in enzymology* **276**, 307–326
28. Storoni, L. C., McCoy, A. J. and Read, R. J. (2004) *Acta Crystallogr D Biol Crystallogr* **60**, 432-438
29. Emsley, P. and Cowtan, K. (2004) *Acta Crystallogr D Biol Crystallogr* **60**, 2126-2132
30. Murshudov, G. N., Vagin, A. A. and Dodson, E. J. (1997) *Acta Crystallogr D Biol Crystallogr* **53**, 240-255
31. Hooft, R. W. and Vriend, G. (1996) *J Mol Graph* **14**, 168-172
32. Humphrey, W., Dalke, A. and Schulten, K. (1996) *J Mol Graph* **14**, 33-8, 27-8
33. Arnold, K., Bordoli, L., Kopp, J. and Schwede, T. (2006) *Bioinformatics* **22**, 195-201

34. Phillips, J. C., Braun, R., Wang, W., Gumbart, J., Tajkhorshid, E., Villa, E., Chipot, C., Skeel, R. D., Kale, L. and Schulten, K. (2005) *J Comput Chem* **26**, 1781-1802
35. MacKerell, J., AD, Brooks, B., Brooks, I. I. I., CL, Nilsson, L., Roux, B., Won, Y. and Karplus, M. (1998) *The encyclopedia of computational chemistry* **1**, 271–277
36. Jorgensen, W. L., Chandrasekhar, J., Madura, J. D., Impey, R. W. and Klein, M. L. (1983) *The Journal of Chemical Physics* **79**, 926
37. Essmann, U., Perera, L., Berkowitz, M. L., Darden, T., Lee, H. and Pedersen, L. G. (1995) *Journal of Chemical Physics* **103**, 8577–8593
38. Weiss, M. S. (2001) *J Appl Crystallogr* **34**, 130-135
39. Davis, I. W., Murray, L. W., Richardson, J. S. and Richardson, D. C. (2004) *Nucleic Acids Res* **32**, W615-9

FIGURE 1

A

B

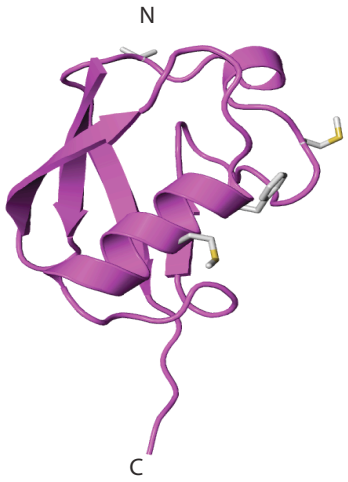

C

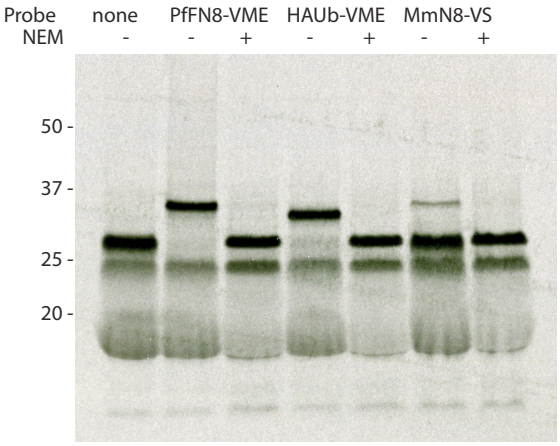

D

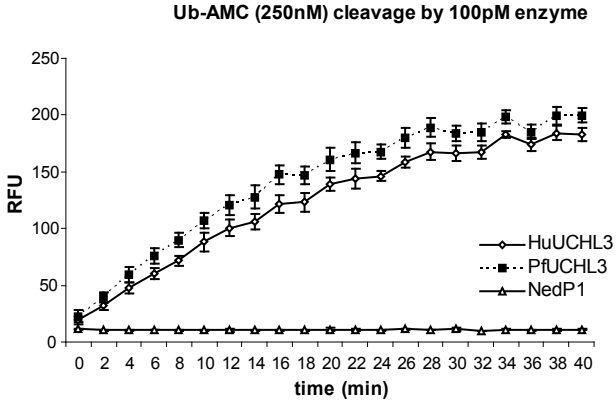

E

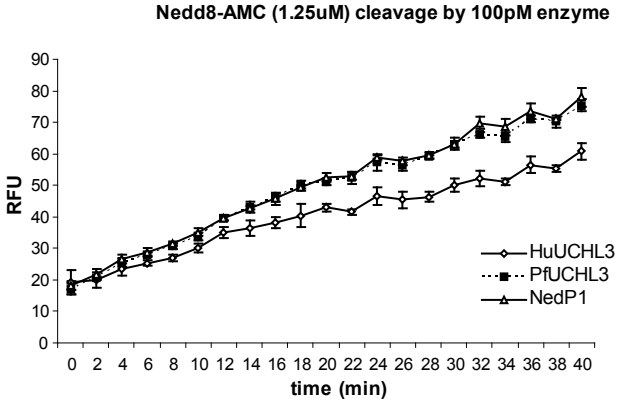

FIGURE 2

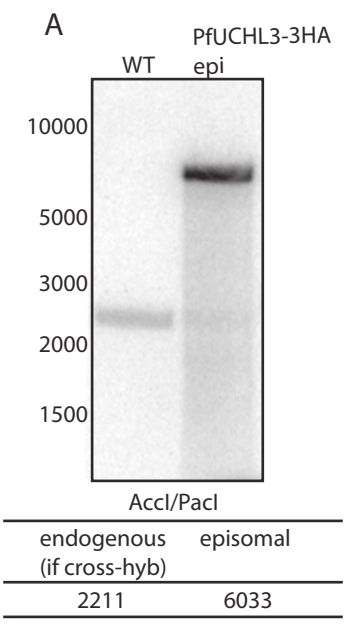
A
PfUCHL3-3HA
WT
epi
10000
5000
3000
2000
1500
AccI/PacI
endogenous
(if cross-hyb)
episomal
2211
6033

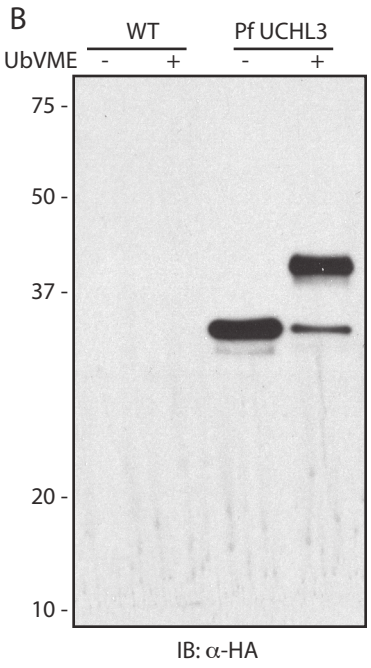
B
WT
Pf UCHL3
UbVME
-
+
-
+
75 -
50 -
37 -
20 -
10 -
IB: α-HA

FIGURE 3

A

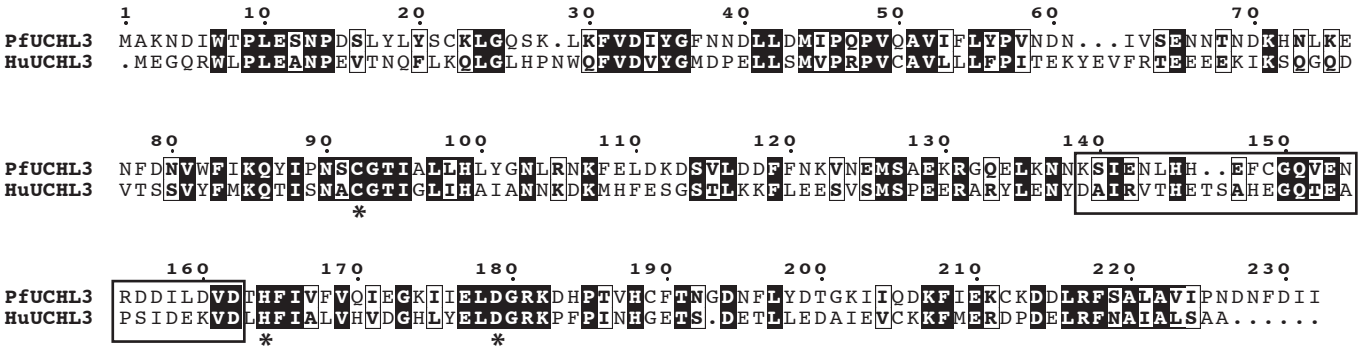
PfUCHL3 MAKNDIWTPLESNPDSLYLYSCKLGQSK.LKFVDIYGFNNDLLDMIPQPVQAVIFLYPVNDN...IVSENNTNDKHNLKE
HuUCHL3 .MEGQRWLPLEANPEVTNQFLKQLGLHPNWQFVDVYGMDPELLSMVPRPVCAVLLLFPITEKYEVFRTEEEEKIKSQGQD
PfUCHL3 NFDNVWFIKQYIPNSCGTIALLHLYGNLRNKFELDKDSVLDDFFNKVNEMSAEKRGQELKNNKSIENLHH..EFCGQVEN
HuUCHL3 VTSSVYFMKQTISNACGTIGLIHAIANNKDKMHFESGSTLKKFLEESVSMSPEERARYLENYDAIRVTHETSAHEGQTEA
PfUCHL3 RDDILDVDTHFIVFVQIEGKIIELDGRKDHPTVHCFTNGDNFLYDTGKIIQDKFIEKCKDDLRFSALAVIPNDNFDII
HuUCHL3 PSIDEKVDLHFIALVHVDGHLYELDGRKPFPINHGETS.DETLLEDAIEVCKKFMERDPDELRFNAIALSAA......

B


HsUb MQIFVKTLTGKTITLEVEPSDTIENVKAKIQDKEGIPPDQQRLIFAGKQLEDGRTLSDYNIQKESTLHLVLRLRGG
PfNedd8 MQILVKTLTGKRQSFNFEPSSSVFQIKMAIEEREGIDAKQIRLIYSGKQMHDDMKLSDYRVVPGSTVHMILQLRGG

FIGURE 4

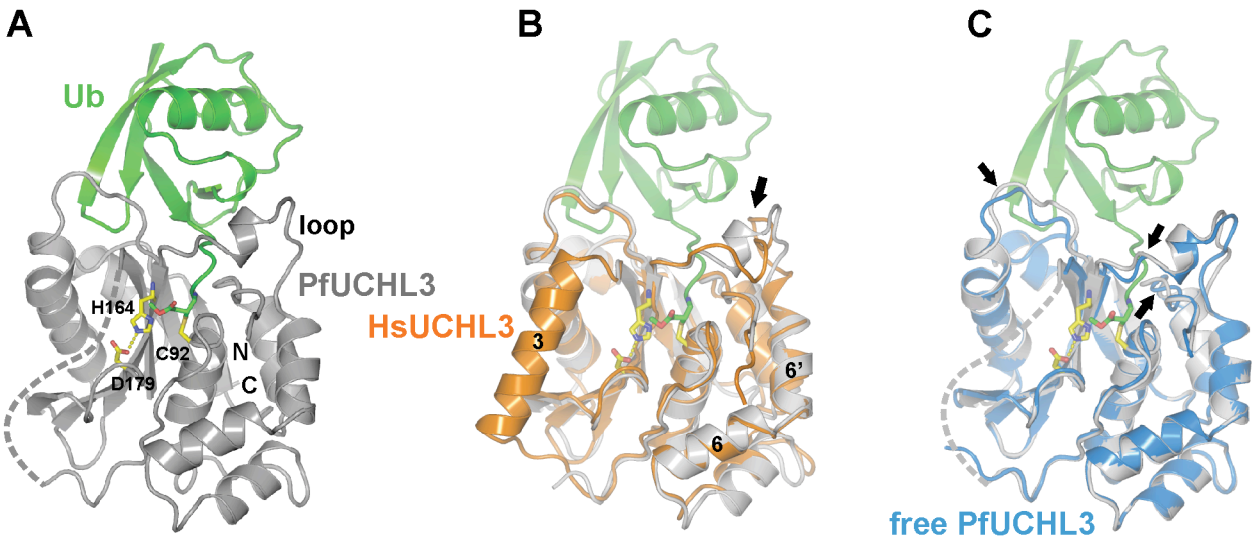
A
Ub
loop
PfUCHL3
H164
C92
D179
N
C
B
HsUCHL3
3
6'
6
C
free PfUCHL3

FIGURE 5

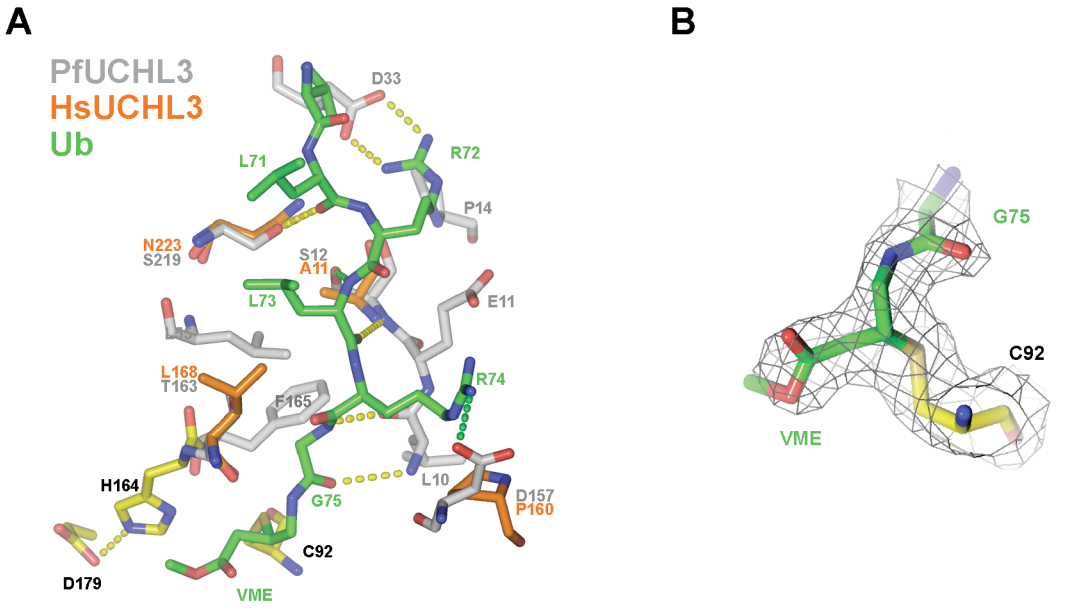
A
PfUCHL3
HsUCHL3
Ub
D33
R72
L71
P14
N223
S219
S12
A11
L73
E11
L168
T163
R74
F165
H164
L10
G75
D157
P160
C92
D179
VME
B
G75
C92
VME

FIGURE 6

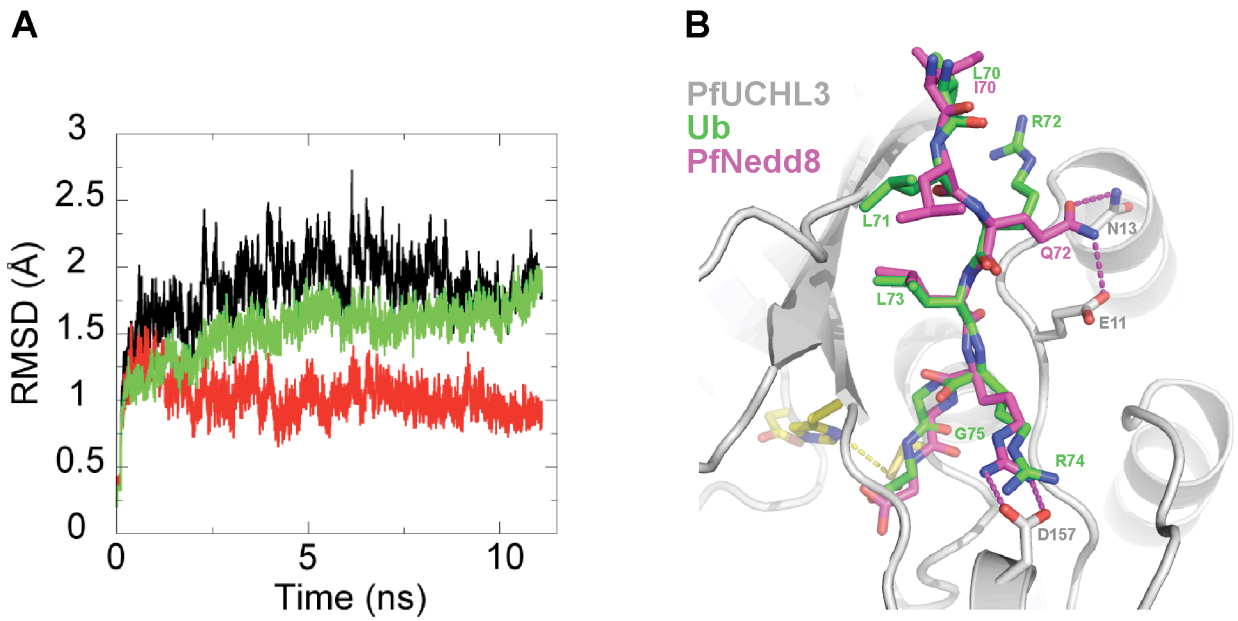
A
RMSD (Å)
3
2.5
2
1.5
1
0.5
0
0
5
10
Time (ns)
B
PfUCHL3
Ub
PfNedd8
L70
I70
R72
L71
N13
Q72
L73
E11
G75
R74
D157